Dyes and Pigments 125 (2016) 27–35

Contents lists available at ScienceDirect

Dyes and Pigments

journal homepage: www.elsevier.com/locate/dyepig

DPP containing D–π–A organic dyes toward highly efficient dye-sensitized solar cells

Kuo Yuan Chiu [a], Venkatesan Govindan [b], Ling-Chuan Lin [c], Shin-Han Huang [c], Jia-Cheng Hu [b], Kun-Mu Lee [a, c, **], Hui-Hsu Gavin Tsai [b, ***], Sheng-Hsiung Chang [a, ****], Chun-Guey Wu [a, b, *]

[a] Research Center for New Generation Photovoltaics, National Central University, No. 300, Zhongda Rd., Zhongli City, Taoyuan 320, Taiwan
[b] Department of Chemistry, National Central University, No. 300, Zhongda Rd., Zhongli City, Taoyuan 320, Taiwan
[c] Department of Chemical and Materials Engineering, National Central University, No. 300, Zhongda Rd., Zhongli City, Taoyuan 320, Taiwan

ARTICLE INFO

Article history:
Received 11 August 2015
Accepted 28 September 2015
Available online 9 October 2015

Keywords:
Dye-sensitized solar cell
Organic
DPP
D-π-A dye
Theoretic calculation
High efficiency

ABSTRACT

Two diketopyrrolopyrrole (DPP) containing D–π–A organic dyes, named as TEDBn and TEDTh were prepared. Their optical, electrochemical and photophysical properties were investigated and their application in dye-sensitized solar cells (DSCs) was demonstrated. The broaden absorption and low-energy λ_{max} of DPP containing dyes were contributed from DPP bridge and EDOT π-conjugated moiety. Compared to TEDTh, TEDBn has smaller absorption coefficient and higher optical bandgap. Nevertheless the power conversion efficiency (PCE) of TEDBn based DSC is 7.2% which is larger than that of TEDTh based DSC and 90% of N719 based cell. The higher PCE of TEDBn based device originates from both higher open-circuit voltage (V_{OC}) and short-circuit current (J_{SC}). Femtosecond time-resolved photoluminescence data show that the electron injection at TEDBn/TiO_2 is more efficient than that at TEDTh/TiO_2 interface, resulting in higher J_{SC} (and IPCE) of TEDBn based DSC. Density function theory (DFT) calculations revealed that TEDBn is a linear structure which leads to higher dye loading on TiO_2 than TEDTh which featured a bend conformation, better TiO_2 surface coverage, resulting in larger V_{OC}. Therefore, the overall efficiency of the cell sensitized by TEDBn is better than that the devices based on TEDTh.

1. Introduction

Metal-free organic dyes have been extensively developed for dye-sensitized solar cells (DSCs) owing to their high absorption coefficient and abundance of the resources. Organic dye used to have donor–π bridge–acceptor (D–π–A) configuration in the main chain [1–17] and triarylamine and cyanoacetic acid were used as donor and acceptor moieties, respectively. Various π-conjugated linkers had been used to construct the high performance D–π–A sensitizers for DSC. Diketopyrrolopyrrole (DPP) pigment with a conjugated bicyclic planar structure and the electron-withdrawing characteristics is one of the widely used π-conjugated units in the D–π–A organic dyes due to its excellent photochemical, mechanical and thermal stability as well as high carrier mobility [18–27]. The photovoltaic performance of DPP based sensitizer has been greatly improved since the dye was first reported by Tian et al. in 2010 [22]. Combining a suitable donor group and asymmetric DPP unit, DPP based dye was proved to be an excellent sensitizer for high efficiency DSCs [24–27]. The length of the donor group in DPP containing dyes also affects their optical property and therefore the photovoltaic performance [9]. For example, symmetric phenyl–DPP dyes have high optical bandgap because the phenyl spacers will lower the HOMO energy level [22]. The optical bandgap of the DPP dyes decreased when the phenyl unit is replaced by thienyl moieties [22]. Furthermore, the V_{OC} of DPP dye sensitized devices can be improved by the structure modification such as the dyes' aggregation can be suppressed by engineering the alkyl chain in the DPP moieties, resulting in a high PEC [11].

* Corresponding author. Department of Chemistry, National Central University, No. 300, Zhongda Rd., Zhongli City, Taoyuan 320, Taiwan.
** Corresponding author. Research Center for New Generation Photovoltaics, National Central University, No. 300, Zhongda Rd., Zhongli City, Taoyuan 320, Taiwan.
*** Corresponding author.
**** Corresponding author.
E-mail addresses: kmlee@cc.ncu.edu.tw (K.-M. Lee), hhtsai@cc.ncu.edu.tw (H.-H. Gavin Tsai), shchang@ncu.edu.tw (S.-H. Chang), t610002@cc.ncu.edu.tw (C.-G. Wu).

http://dx.doi.org/10.1016/j.dyepig.2015.09.033
0143-7208/

In this study we designed and synthesis two asymmetric metal-free organic dyes TEDBn and TEDTh (the structures were displayed in Scheme 1) using DPP as a part of the π-conjugated bridge, 4,4′-Ditolylaniline as the donor and cyanoacetic acid as the acceptor and anchoring group. Phenyl and thienyl spacers were individually inserted between the anchoring group and the DPP core to form two D–π–A dyes. Under 1 Sun (100 mW/cm^2, AM 1.5 G) illumination, TEDBn sensitized DSC achieves the high PCE of 7.2% which is *ca.* 90% of that for the cell based on N719 dye.

2. Experimental

2.1. Materials and physicochemical study

All chemicals used were obtained from the commercial resources and used as received unless specified. HPLC grade CH_2Cl_2 was purchased from ACROS and was distilled from CaH_2 under an argon (Ar) atmosphere for electrochemical use. Tetra-*n*-butylammonium hexafluorophosphate ($TBAPF_6$) was recrystallized from ethanol twice and then stored in a desiccator. ^1H NMR and ^{13}C NMR spectra were recorded with a Bruker 300 MHz or Bruker 500 MHz NMR spectrometer using $CDCl_3$ as a solvent. FAB-MS spectra were obtained using JMS-700 HRMS. UV/Vis absorption and emission spectra were measured using a Cary 300 Bio spectrometer and FluoroMax-4 spectrofluorometer (HORIBA JOBIN YVON), respectively. Elemental analyses were carried out with a Heraeus CHN–O–S Rapid-F002 analysis system. Electrochemistry was conducted using a three-electrode cell with BAS glassy carbon working electrode (GCE, area = 0.07 cm^2). The glassy carbon electrode was polished with 0.05 μm alumina on Buehler felt pads and was ultrasonicated for 2 min to remove the alumina residue. A platinum wire was used as the auxiliary electrode. A home-made Ag/AgCl, KCl (sat'd) is the reference electrode. The supporting electrolyte is 0.1 M tetrabutylammonium hexafluorophosphate ($TBAPF_6$) in CH_2Cl_2. The square-wave voltammograms (frequency: 25 Hz; step potential: 0.0051 V; amplitude: 0.01995 V) were recorded using a potentiostat/galvanostat (PGSTAT 30, Autolab, Eco-Chemie, the Netherlands) and ferrocene was used as a calibration standard (+0.54 V versus Ag/AgCl).

2.2. Synthesis of TEDBn and TEDTh

The synthetic route for TEDBn and TEDTh dyes was illustrated in Scheme 1. DPPBn and DPPTh were synthesized according to the previously reports [7,9,10]. The detailed synthesis and characterization of TEDBn and TEDTh can be found in Supporting Information (SI).

2.3. Computational methods

The ground state molecular geometries of TEDBn and TEDTh molecules (in protonated states) in the THF were optimized using Becke's three-parameter exchange function [28], the Lee–Yang–Parr gradient-corrected correlation function (B3LYP) [29], and the 6-31G (d,p) basis set [30], as implemented in the program Gaussian 09 [31]. The conductor-like polarizable continuum model (C-PCM) could account for the solvation effect [32]. All the long alkyl chains were replaced with methyl groups to save computational resources. The UV–Vis spectra of the free molecules in THF were calculated using TD-DFT. The charge transfer excitation properties of the dye molecules are particularly important in DSCs, the coulomb-attenuating method (CAM) [33] was applied [at the TD-CAM-B3LYP/6-31G (d,p) theoretical level] to calculate the UV–Vis spectra. For the excited state calculations, the excited-state geometries of free dyes in THF were optimized at the B3LYP/6-31G (d,p) theoretical level; the fluorescence spectra of free dyes in THF were calculated at the TD-CAM-B3LYP/6-31G (d,p) theoretical level.

To model the experimental properties of the dye molecules adsorbed on TiO_2 thin films, we studied dyes adsorbed on $(TiO_2)_{38}$ clusters. The dye adsorbed was on the anatase (101) surface of the

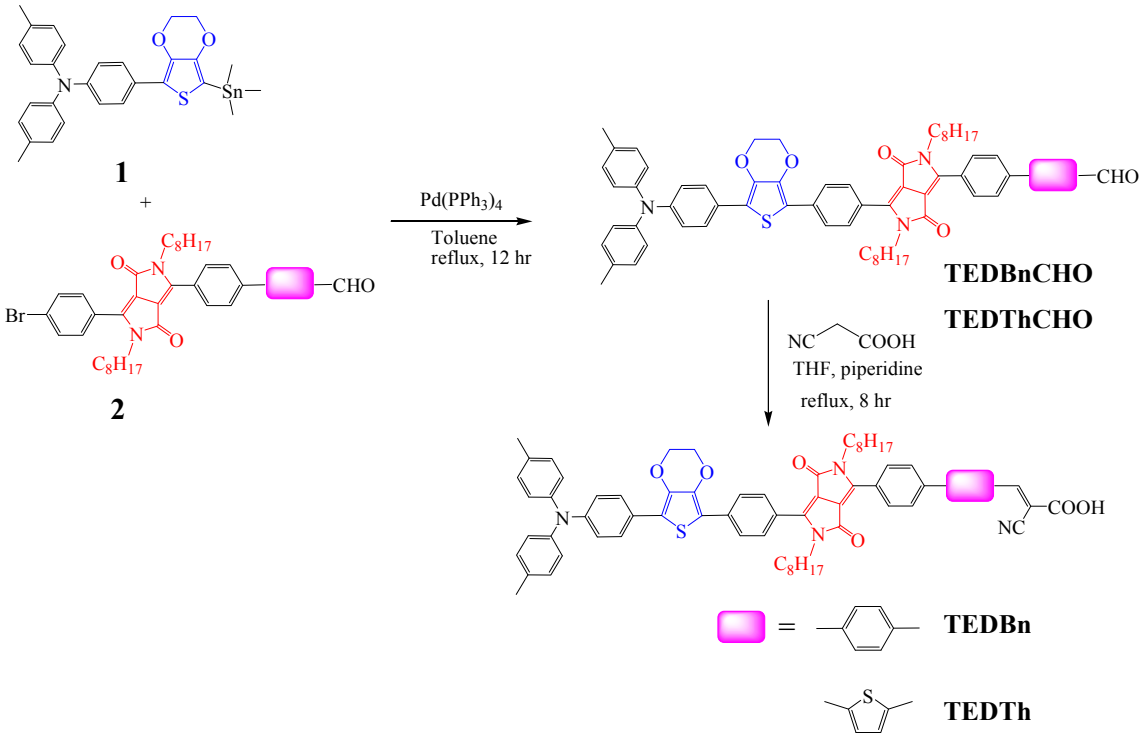

Scheme 1. Synthetic route of DPP dyes.

$(TiO_2)_{38}$ super-cluster [34] in a bidentate manner. Two O atoms of the carboxylic acid are bound to two neighboring five-coordinated Ti atoms (Ti_{5c}) on TiO_2 surface with the proton transferred to the neighboring O atom on TiO_2 (Fig. 1). Perdew–Burke–Ernzerhof (PBE) parameterization of the generalized gradient approximation (GGA) [35], in conjunction with the double numerical basis sets with polarization (DNP) [36], was adopted for geometric optimization of the dye–$(TiO_2)_{38}$ complexes as implemented in the DMol software package [37,38]. Gaussian 09 default optimization and all-electron core treatment were used for geometric optimization of the dye–$(TiO_2)_{38}$ systems. Finally, the UV–Vis spectra of the studied dye–$(TiO_2)_{38}$ complexes obtained using the TD-CAM-B3LYP/6-31G (d,p) method with Gaussian 09 in THF (modeled by C-PCM) were calculated. Electron density difference maps (EDDMs) were generated using GaussSum (v. 2.2.6) [39]. The EDDMs representing the electronic transitions revealed the changes in electron density before and after the transitions.

2.4. Femtosecond time-resolved photoluminescence (FTR-PL)

To understand the photoexcited dynamics of the electrons in TEDTh, TEDBn, TEDTh/TiO_2, and TEDBn/TiO_2, the FTR-PL was measured by the sum-frequency technique (FluoMax, IB Photonics Ltd.). The dye dissolved in (adsorbed on) THF solvent (or adsorbed on TiO_2) was pumped with a wavelength of 420 nm. To prevent laser-induced thermal effects, the diameter of the spot size on the sample was increased to 300 μm and the excitation power was reduced to 4 mW. In order to resolve the exciton dynamics, the time-dependent photoluminescence is fitted in an appropriate exponentially decaying function [40].

2.5. Device fabrication and photovoltaic performance test

Anatase TiO_2 nanoparticles (NP) (*ca.* 20 nm diameter) used in this study were prepared in a Ti based autoclave as reported previously [41]. The detailed device fabrication and photovoltaic performance test are described in the SI.

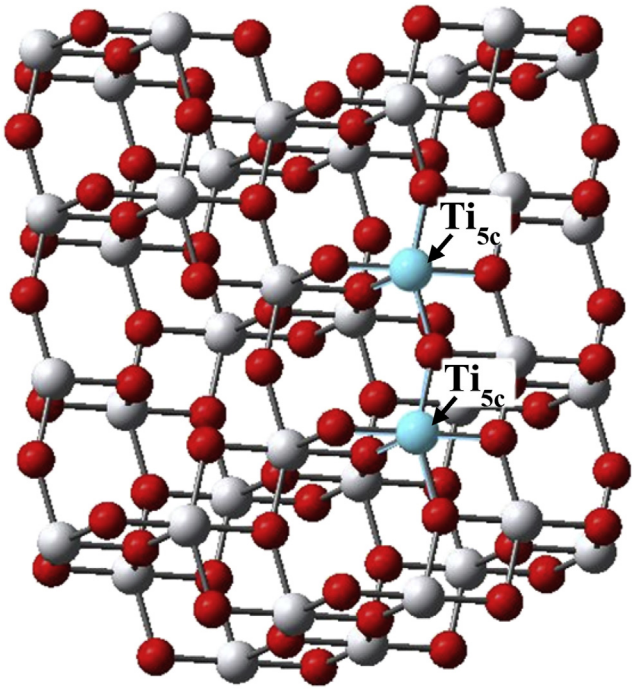

Fig. 1. The $(TiO_2)_{38}$ cluster with an anatase (101) surface used in the calculation highlighting two five-coordinated Ti atoms.

3. Results and discussion

Two DPP-containing dyes (TEDBn and TEDTh) show broad absorption spectra with two absorption bands covering a wide wavelength range from 300 to 700 nm in THF (Fig. 2). For TEDBn, the absorption peak at 343 nm is contributed from the donor group and the peak of 520 nm is assigned to the intramolecular charge transfer (ICT) band. The absorption spectrum of TEDTh dye also shows two peaks at wavelengths of 382 and 530 nm. There is significant red-shift (~40 nm) in the short-wavelength peak (λ_{max}, 382 nm) of TEDTh dye compared to TEDBn dye, because a thienyl ring is attached to the anchoring group of TEDTh dye. However, there is only a slight red-shift (10 nm) in the ICT band of the TEDTh dye compared to that of TEDBn dye since the donor and acceptor for both dyes are the same, similar phenomenon was observed in literature [24]. Moreover, the molar extinction coefficient (ε) of TEDTh (2.25×10^5 M^{-1} cm^{-1} at $\lambda = 382$ nm) is higher than that of TEDBn (1.45×10^5 M^{-1} cm^{-1} at $\lambda = 343$ nm) and both are higher than other DPP containing dyes reported in the previous studies [18–27,42,43]. The photoluminescence (PL) spectra (Fig. 2) reveal that the emission maxima (λ_{EM}) for TEDBn and TEDTh dyes in THF are 569 nm and 587 nm, respectively. The Stokes shift (the wavelength difference between the λ_{max} of the absorption and the λ_{EM} of the emission peak) of the dye is related to the efficiency of the

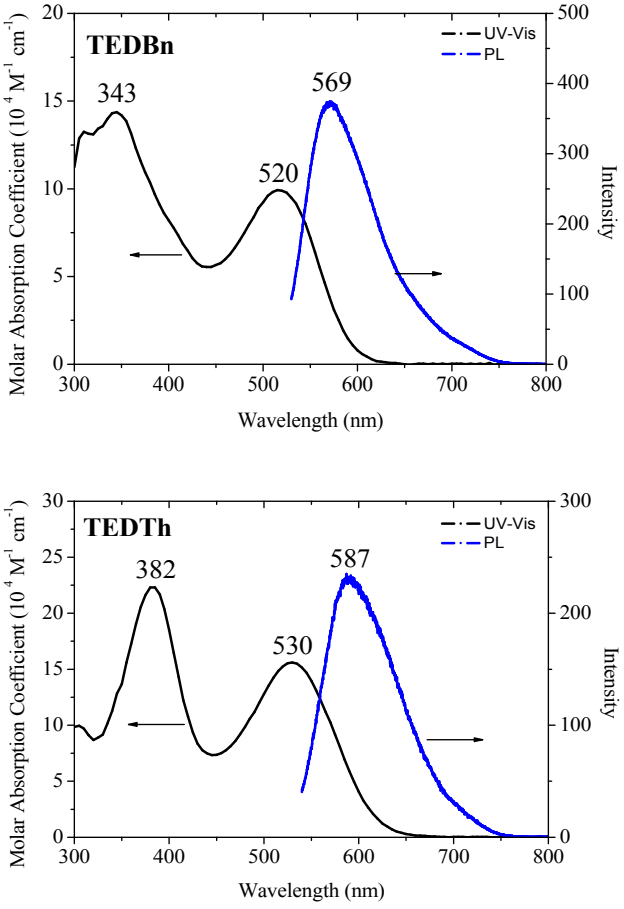

Fig. 2. UV–Vis absorption (black line) and emission (blue line) spectra of TEDBn and TEDTh in THF. (For interpretation of the references to color in this figure legend, the reader is referred to the web version of this article.)

electron injection from dye to TiO_2, which will be discussed more in the later paragraph.

TD-DFT calculations are performed to calculate the optical data of these two dyes and the results as well as those obtained from the experimental observations are listed in Table 1. The calculated ICT absorption bands for TEDBn and TEDTh are 501 and 520 nm, respectively, which are in good agreement with the experimental data. The ICT absorption bands of TEDBn and TEDTh involve four molecular orbitals HOMO − 1 and HOMO to LUMO and LUMO + 1 with strong mixing of these four transitions. In particular, HOMO − 1 to LUMO and HOMO to LUMO transitions are the two main transitions. The calculated HOMO − 1, HOMO, LUMO and LUMO + 1 orbitals for TEDBn and TEDTh dyes are displayed in Figs. S1 and S2, SI. For both dye molecules the electron density in HOMO − 1 is mainly distributed on DPP moieties while the electron density of HOMO is mainly located on ditolylaniline-EDOT moieties. The electron density of LUMO and LUMO + 1 is mainly distributed on DPP-phenyl-phenyl (thiophene)-acceptor moieties. Table 2 summarizes the electron density on every moieties of TEDBn and TEDTh in THF before (where the electron density is coming from) and after (where the electron density is going to) the photo-excitation. The data show that the electron densities of the anchoring groups increased by *ca.* 24% for both dyes indicating that in THF the electron density of TEDBn and TEDTh is transferred moderately toward the anchoring groups upon excitation.

The first oxidation potential (E_{ox}) of the dye was measured by square wave voltammetry (SWV, Fig. S3, SI) using $TBAPF_6/CH_2Cl_2$ as an electrolyte, which corresponds to the HOMO level. The E_{ox} of TEDBn and TEDTh were +0.70 and +0.69 V vs Ag/AgCl (+0.90 and +0.89 V vs NHE), respectively. The HOMO level for TEDBn and TEDTh is very close and both are higher than those of DPP containing dyes studied previously [11,20–27] due to the contribution of the strong donor EDOT unit. The values of E_{ox}, for the two dyes were more positive than the redox potential of I^-/I_3^- couple (~0.4 V vs NHE) which is employed as an electrolyte in the DSC devices in this study. The LUMO levels were calculated by HOMO + E_{0-0}, where E_{0-0} is the optical transition energy of the dyes estimated from the onset value of the absorption spectra. The E_{0-0} of TEDBn (TEDTh) is 1.93 eV (1.81 eV), yielding a LUMO of −3.47 eV (−3.58 eV). Compared with other DPP containing dyes reported previously [24–27,44,45], the insertion of an EDOT moiety between ditolylaniline and DPP unit would lift not only the HOMO level but also the LUMO level because of EDOT is an electron donating group. The optical and electrochemical data displayed in Table 3 show that the electron can be injected facilely into TiO_2 conduction band (E_{cb}, *ca.* −0.04 V vs NHE, −3.94 eV vs vacuum) from the photo-excited sensitizers, and the oxidized dyes can be regenerated by I^-/I_3^- redox couple. The result indicates that organic dye containing DPP unit in the back bone would be an efficient sensitizers when applied in DSCs.

Fig. 3 shows the alignment of the calculated energy levels of the TEDBn–$(TiO_2)_{38}$ and TEDTh–$(TiO_2)_{38}$ systems and the difference in the electron density between the ground state and first excited state (EDDM) and the related data were summarized in Table 4. The energy alignment is the combination of the occupied energy level and the TD-DFT calculated excitations spectra proposed by De Angelis and co-workers [46,47]. Interestingly, the EDDM results revealed that the same electron (hot electron, excited electron without thermal relaxation) density (14%) transferred from the dye to $(TiO_2)_{38}$ cluster for both TEDBn–$(TiO_2)_{38}$ and TEDTh–$(TiO_2)_{38}$ systems. The result suggests that the fermi levels of TiO_2 for two dye-adsorbed TiO_2 anodes are similar. The excited state energy level is accordingly calculated to be at −3.47 and −3.57 eV for the lower-energy transitions of the TEDBn–$(TiO_2)_{38}$ and TEDTh–$(TiO_2)_{38}$ systems, respectively. Therefore, the lowest driving forces for electron injection are 0.47 and 0.37 eV for the TEDBn–$(TiO_2)_{38}$ and TEDTh–$(TiO_2)_{38}$ systems, respectively (relative to the energy level of the experimental TiO_2 conduction band (−3.94 eV)). The computed results also indicated that both TEDBn–$(TiO_2)_{38}$ and TEDTh–$(TiO_2)_{38}$ systems have sufficient driving force for the electron injection. Moreover, the TEDBn–$(TiO_2)_{38}$ systems have only a slight larger driving force (0.10 eV) compared to the TEDTh–$(TiO_2)_{38}$ systems, indicating that the electron (cold electron, the excited electron after thermal relaxation) injection rate is larger in the TEDBn–$(TiO_2)_{38}$ system than in the TEDTh–$(TiO_2)_{38}$ system. Therefore the J_{SC} of the corresponding cells will be determined not only by the absorption (the absorption coefficient times dye loading) of the adsorbed dyes but the rate of the electron injects from the excited dye to TiO_2 electrode.

The *J*–*V* curves of the two dye-sensitized DSCs are shown in Fig. S4 (a), SI and the detailed photovoltaic parameters were summarized in Table 5. The photocurrent (J_{SC}) of the TEDBn based DSC is close to that of TEDTh based DSC. The J_{SC} value is related to the absorption coefficient of the dye, dye loading on the TiO_2 electrodes, electron injection from dye to TiO_2, and charge recombination of the devices [40]. The dye loading of the DSC was quantified by immersing the practical TiO_2 anodes in a 0.20 mM THF dye solution, and the concentration difference before and after anode soaking was quantified by optical spectrophotometry [38]. TEDTh has a loading of 2.95×10^{-8} mol cm^{-2} in contrast to that (3.88×10^{-8} mol cm^{-2}) for TEDBn (see Table 5). The lower dye loading of TEDTh can be rationalized at the molecular level from the DFT computations (will be discussed in the following paragraph) which indicates that thienyl containing dye has a more bending conformation, resulting in lower dye loading. Although the dye

Table 1
Experimental (EXP.) and computational electronic absorptions, transition characters, and EDDMs of the DPP-containing dyes in THF.

Dyes	EXP. Calculation				
	λ_{max} (nm)	λ_{max} (nm)	Transitions[a]	EDDM (where the electron density is coming from)	EDDM (where the electron density is going)
TEDBn	520	501	HOMO − 1 → LUMO (39%) HOMO → LUMO (32%) HOMO → LUMO + 1 (10%) HOMO − 1 → LUMO + 1 (10%)	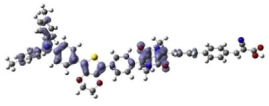	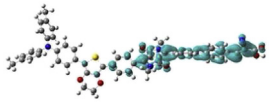
TEDTh	530	520	HOMO − 1 → LUMO (41%) HOMO → LUMO (29%) HOMO → LUMO + 1 (12%) HOMO − 1 → LUMO + 1 (10%)	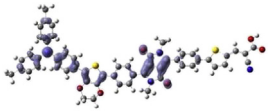	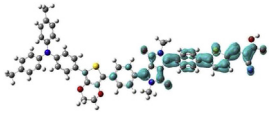

Transitions with a contribution larger than 5% are shown.

Table 2
Characteristics of the electron density for each moiety of TEDBn and TEDTh dyes in THF before and after transition.

Dye	λ_{abs}	Change	Percent contribution (%)							
			Ditolylamine	Ph	EDOT	Ph	DPP	Ph	R[b]	Acceptor
TEDBn[a]	501 nm	Before	27	13	12	8	33	5	1	0
		After	0	2	5	9	32	12	16	24
		Net	−27	−11	−7	+1	−1	+7	+15	+24
TEDTh[a]	520 nm	Before	26	13	12	8	32	5	3	1
		After	0	1	4	8	28	13	21	24
		Net	−26	−12	−8	0	−4	+8	+18	+24

[a] The molecule is classified by different groups, which are arranged in the table from the donor side (ditolylamine) to the acceptor side.
[b] Phenyl for TEDBn and thienyl for TEDTh.

Table 3
Optical and electrochemical data of the two DPP-containing dyes.

	1st $E_{1/2}$ (V vs NHE)	HOMO (eV)[a]	λ_{onset} (nm)	$E_{0\text{-}0}$ (eV)[b]	LUMO (eV)[c]
TEDBn	+0.90	−5.40	655	1.93	−3.47
TEDTh	+0.89	−5.39	670	1.81	−3.58

[a] $FeCp_2^{+/0}$ = +0.50 V (vs Ag/AgCl) in $TBAPF_6/CH_2Cl_2$. The HOMO energy level was calculated from the half-wave potential of the oxidation according to the empirical formula $E_{HOMO} = -(E_{1/2} + 4.5)$ V, assuming the energy level of ferrocene to be −4.5 eV below the vacuum level.
[b] The gap energy (E_{0-0}) was calculated from the onset wavelength of the UV–Vis spectrum according to the empirical formula $E_{gap} = 1240/\lambda_{onset}$.
[c] LUMO = HOMO + E_{0-0}.

loading of TEDBn is 20% higher than TEDPh and the injection rate is also higher, the devices based on these two dyes have similar J_{SC} value. This is because of TEDBn has smaller absorption coefficient compared to TEDTh as the data listed in Table 5.

The V_{OC} of the DSCs based on TEDBn (0.762 V) is higher than that for the cell sensitized with TEDTh (0.711 V). V_{OC} of the DSCs related to the series resistant and charge recombination of the cell. Higher V_{OC} for TEDBn based device may be due to TEDBn has higher dye loading and therefore better TiO_2 protection, less charge recombination. Electrochemical impedance spectroscopy (EIS) under dark was taken to elucidate the difference in TiO_2 surface coverage by these two dyes. The EIS measurement was performed over the frequency range from 10 mHz to 65 kHz at the applied bias voltage set at −0.76 V. The Nyquist plots (Fig. S4 (b), SI) show two semicircles which are assigned to the electrochemical reaction at the Pt/electrolyte interface, charge transfer at the TiO_2/dye/electrolyte interface, and the Warburg diffusion process of the electrolyte (I^-/I_3^-). In general the conventional diffusion resistance of the redox couple is greatly overlapped by the charge-transfer resistance because of the relatively short length available for I^- diffusion within the thin spacer and owing to the low viscosity of the solvents used in the electrolyte. TEDBn based device has higher TiO_2/dye/electrolyte interface resistance, indicating the TEDBn dyed TiO_2 has better surface protection and therefore has less electron recombination results in larger open-circuit voltage as general observed in DSCs [48].

The dye loading of a DSC may relate to the conformation of dye molecule. The conformation of TEDBn and TEDTh adsorbed on TiO_2 are investigated by calculating the length of the projection of dyes. Fig. 4 displays the calculated configurations of TEDBn and TEDTh when adsorbed on $(TiO_2)_{38}$ clusters. The molecular lengths of TEDBn and TEDTh are 2.86 nm and 2.81 nm, respectively. We defined the length of the projection as the distance between the coordinates of the C atoms of carboxylic acid and the coordinates of the N atoms on ditolylaniline projected on TiO_2 surfaces. The calculated projection lengths for TEDBn and TEDTh are 8.13 and 8.77 Å, respectively. The longer projection length of TEDTh suggests that one TEDTh molecule can occupy more TiO_2 surface than one TEDBn molecule. Thus, TEDTh will have lower loading on TiO_2 than TEDBn, consistent with the experiment data. The bending structure of TEDTh originated from the chemical connectivity between the thienyl ring and its two neighboring moieties at the 2,5-positions. On the other hand, the phenyl ring in TEDBn is chemically connected to its two neighboring moieties at the *para* positions, leading to a more linear geometry. Higher dye loading and linear molecular conformation results in better TiO_2 coverage, less charge recombination, therefore higher V_{OC}. IPCE spectra displayed in Fig. S4 (c) (Supporting information) reveal that TEDBn based DSC has narrower IPCE spectrum compared to TEDTh sensitized device, which is consistent with the narrower absorption profile of TEDBn dye (see Fig. 2). Nevertheless TEDBn based cell has IPCE value higher than that for the cell sensitized by TEDTh at wavelength of 350–650 nm, due to TEDBn has higher dye loading and less charge recombination. As a result, the J_{SC} values for the devices sensitized by the two dyes are very close.

Another parameter affects the J_{SC} of a DSC is the efficiency of the "cold" electron injection from dye to TiO_2. In the previous paragraphs we had shown the efficiency of the "hot" electron injection from dye to TiO_2 by calculation. A simple method to investigate the "cold" electron injection efficiency is by probing the exciton binding energy of the dye molecule [49]. The Stokes shift (related to the exciton binding energy) of the dye can be calculated by taking the wavelength difference between the λ_{max} of the absorption and the λ_{EM} of the emission peak shown in Fig. 2. The Stokes shift of TEDBn (49 nm) is smaller than that of TEDTh (57 nm), indicating that TEDBn has weaker excitons binding energy which could result in more efficient electron injection for TEDBn dye to TiO_2 anode. The intrinsic "cold" exciton lifetime of dye in THF can be measured with the time-resolved PL of TEDBn and TEDTh using the sum-frequency technique as shown in Fig. S5, SI. To obtain the relaxation times, the experimental results are fitted in a 2-constant exponentially decaying function as follows:

$$I_{PL} = A_{ee}e^{-t/\tau_{ee}} + A_e e^{-t/\tau_e}, \quad (1)$$

where A_{ee} is the amplitude of "cold" exciton–exciton annihilation; A_e is the amplitude of "cold" excitons, τ_{ee} is the time of exciton–exciton annihilation, and τ_e is the lifetime of "cold" excitons. The fitted results are listed in Table 6. The "cold" exciton lifetimes of TEDBn and TEDTh are 602 ps and 441 ps, respectively. The exciton

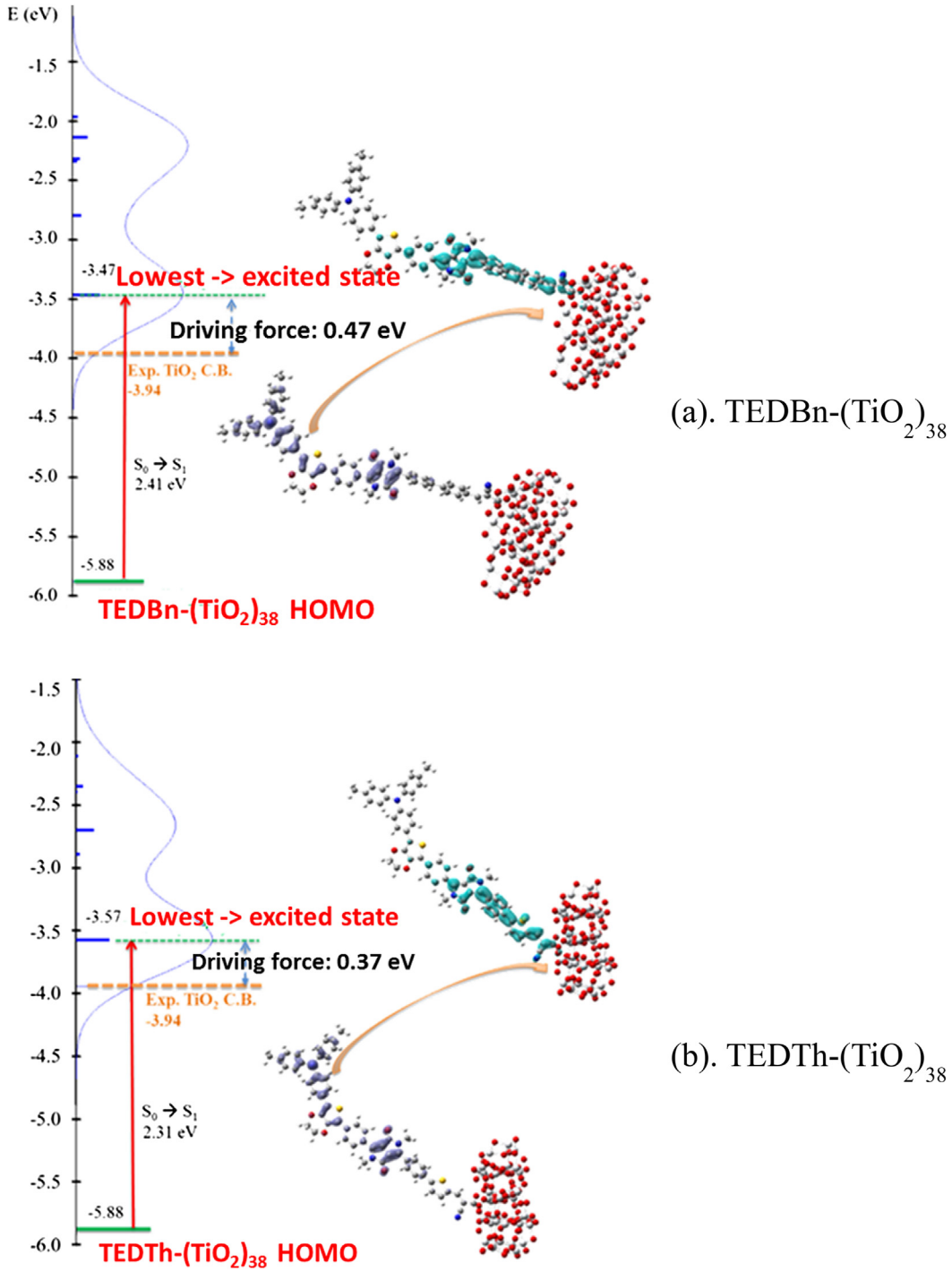

Fig. 3. Alignment of the ground and excited state energy levels for the dye-$(TiO_2)_{38}$ systems and the EDDMs for the dye-$(TiO_2)_{38}$ systems, before (the purple indicates where the electron density is coming from) and after (the cyan indicates where the electron density is going) photo-excitation. Orange dashed and green dashed lines indicate the edge of the experimental TiO_2 conduction band (CB) and the calculated HOMO energy levels of the dye-$(TiO_2)_{38}$ systems: (a) TEDBn-$(TiO_2)_{38}$; (b) TEDTh-$(TiO_2)_{38}$ systems. (For interpretation of the references to color in this figure legend, the reader is referred to the web version of this article.)

Table 4
Characteristics of the electron density for each moiety of TEDBn and TEDTh dyes adsorbed on TiO_2 before and after transition.

Dye	λ_{abs}	Change	Percent contribution (%)								
			Ditolylamine	Ph	EDOT	Ph	DPP	Ph	R[b]	Acceptor	$(TiO_2)_{38}$
TEDBn–$(TiO_2)_{38}$[a]	514 nm	Before	28	14	13	8	31	4	1	0	0
	$f = 1.86$	After	0	1	5	11	37	12	9	11	14
		Net	−28	−13	−8	+3	+6	+8	+8	+11	+14
TEDTh–$(TiO_2)_{38}$[a]	536 nm	Before	27	13	11	7	31	6	3	1	0
	$f = 2.20$	After	0	1	3	7	31	15	15	15	14
		Net	−27	−12	−8	0	−1	+9	+12	+14	+14

[a] The molecule is classified by different groups, which are arranged in the table from the donor side (ditolylamine) to the acceptor side.
[b] Phenyl for TEDBn and thienyl for TEDTh.

Table 5
Photovoltaic performance of DSCs sensitized with TEDBn, TEDTh and N719, dye loading and the absorption (Abs) of dye adsorbed TiO_2 anodes.

Dye	J_{SC} (mA/cm^2)	V_{OC} (V)	FF	η (%)	Dye loading (10^{-8} mol cm^{-2})	ε (10^5 M^{-1} cm^{-1})	Abs
TEDBn	12.7	0.762	0.74	7.2	3.88	1.45	5.63
TEDTh	12.3	0.711	0.76	6.6	2.95	2.25	6.64
N719	13.4	0.799	0.73	7.8	–	–	–

Abs = dye loading × absorption coefficient (ε).
Electrolyte: 0.6 M BMII, 0.1 M LiI, 0.05 M I_2, 0.1 M GuNCS, 0.5 M TBP in dried acetonitrile.

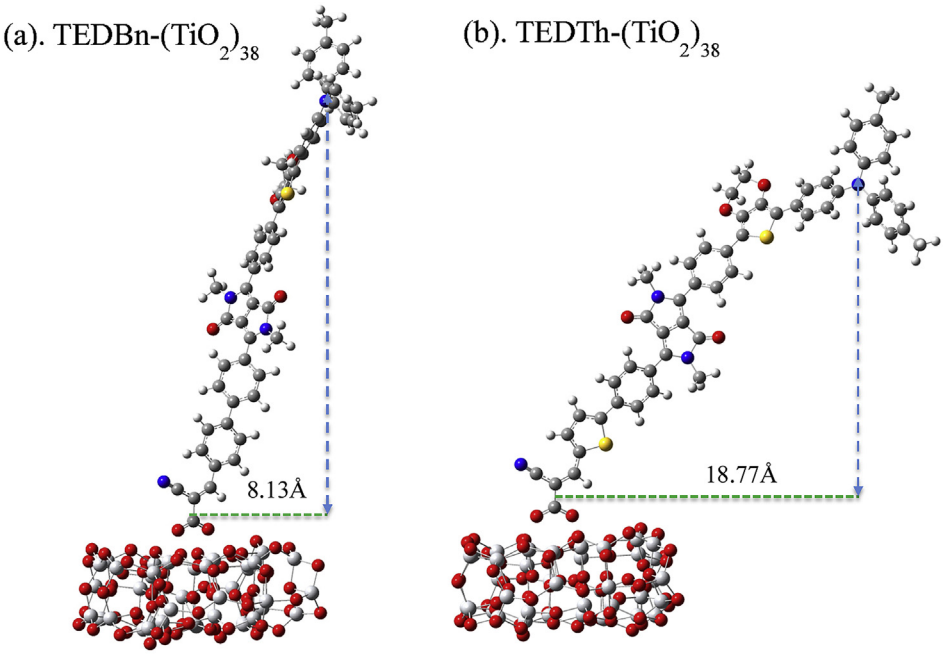

Fig. 4. The length of the projection of TEDBn and TEDTh dyes adsorbed on TiO_2 surface.

lifetime in the dye is inversely proportional to the exciton binding energy which is related to the ability of electron injection from dye to TiO_2 anode in dye-sensitized solar cells. The lifetime of "cold" excitons is consistent with the exciton binding energy obtained from the Stokes shift of the dye molecules in THF, which suggests that TEDBn having weaker exciton binding energy and longer exciton lifetime will have higher electron injection efficiency when adsorbed on TiO_2 compared to TEDTh.

In order to get the direct evidence of the electron injection from the dye to TiO_2, the time-resolved PL of dye adsorbed TiO_2 were measured and displayed in Fig. 5. To obtain the relaxation time, the experimental results are fitted into a 3-constant exponentially decaying function as follows:

$$I_{PL} = A_i e^{-t/\tau_i} + A_{ee} e^{-t/\tau_{ee}} + A_e e^{-t/\tau_e}, \quad (2)$$

where A_i is the amplitude of the electron injection, A_{ee} is the amplitude of exciton–exciton annihilation, A_e is the amplitude of the residual exciton, τ_i is the electron injection time, τ_e is the exciton–exciton annihilation time, and τ_e is the exciton lifetime. The "cold" electron injection efficiency can be evaluated by

Table 6
Exciton–exciton annihilation time (τ_{ee}) and exciton lifetime (τ_e) for the two DPP-containing dyes dissolved in the THF and Electron injection time (τ_i), exciton–exciton annihilation time (τ_{ee}), exciton lifetime (τ_e) and electron injection efficiency (η) for the two DPP-containing dyes adsorbed on TiO_2.

Dye in THF	A_{ee}	τ_{ee} (ps)	A_e	τ_e (ps)
TEDBn	0.5	220	0.5	602
TEDTh	0.51	114	0.49	441

Dye adsorbed in TiO_2 film	A_i	τ_i (ps)	A_{ee}	τ_{ee} (ps)	A_e	τ_e (ps)	η (%)	A_i	τ_i (ps)
TEDBn	0.55	1.06	0.31	5.36	0.14	35.81	97.1	0.55	1.06
TEDTh	0.61	1.67	0.26	9.52	0.13	40.30	96.0	0.61	1.67

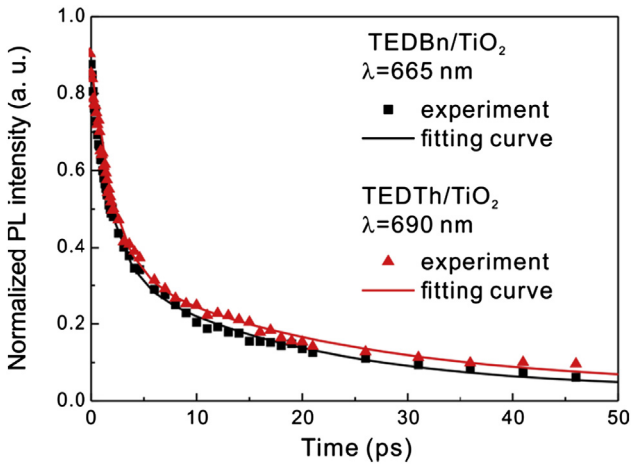

Fig. 5. Time-resolved photoluminescence of TEDBn/TiO_2 and TEDTh/TiO_2.

$\eta = 1/\tau_i/(1/\tau_i + 1/\tau_e)$. The tree time constants and the estimated "cold" electron injection efficiency are also listed in Table 6. The experimental results show that the "cold" electron injection efficiency at TEDBn/TiO_2 (η ~ 97%) is only slightly better than that (η ~ 96%) at TEDTh/TiO_2 and both dye has very high electron injection efficiency.

4. Conclusion

We have revealed that DPP-containing organic sensitizers can achieve excellent photovoltaic performance. The density function theory (DFT) calculation shows that DPP increases the intramolecular charge transfer to enhance the absorption coefficient of the molecule. TEDTh dye has the record-high molar extinction coefficient of $2.25 \times 10^5\ M^{-1}\ cm^{-1}$ at $\lambda = 530$ nm, contributed from ditolylaniline, EDOT, and DPP moieties. The optical bandgap of DPP-containing dye can be reduced through the insertion of thienyl spacer between the anchoring groups and DPP core. However, the thienyl in the anchoring group significantly affects the conformation of the molecule, results in bending structure and therefore low dye loading on TiO_2 anode. On the other hand, TEDBn dye containing phenyl spacer, although has low absorption coefficient, is a linear geometry therefore has high dye loading. Nevertheless, the overall absorption (dye loading times absorption coefficient) of TEDBn adsorbed TiO_2 is still lower than that of TEDTh adsorbed TiO_2. Photon dynamic studies show that comparing to TEDTh, the exciton of TEDBn has lower binding energy and longer lifetime and therefore has higher electron injection efficiency when adsorbed on TiO_2. Therefore the J_{SC} values for the DSCs based on TEDBn and TEDTh dyes are very close. Nevertheless high dye loading of TiO_2 forms a good surface protection, the corresponding cell has less charge recombination, therefore high V_{OC}. Under 1 Sun (100 mW/cm^2, AM 1.5 G) TEDBn based DSC exhibits a good PCE of 7.2% which is 90% of N719 based cell. The results demonstrate that DPP containing D–π–A dyes has a great potential to be the sensitizers for the high-performance DSCs.

Acknowledgment

Financial support from the Ministry of Science and Technology (MOST), Taiwan, ROC (grand number: NSC101-2113-M-008-008-MY3), is gratefully acknowledged. The devices fabrication and photovoltaic parameters measurements were carried out in Advanced Laboratory of Accommodation and Research for Organic Photovoltaics, MOST, Taiwan, ROC.

Appendix A. Supporting information

Supporting information related to this article can be found at http://dx.doi.org/10.1016/j.dyepig.2015.09.033.

References

[1] Koumura N, Wang ZS, Mori S, Miyashita M, Suzuki E, Hara K. Alkyl-functionalized organic dyes for efficient molecular photovoltaics. J Am Chem Soc 2006;128:14256–5257.
[2] Kim S, Lee JK, Kang SO, Ko J, Yum JH, Fantacci A, et al. Molecular engineering of organic sensitizers for solar cell applications. J Am Chem Soc 2006;128:16701–7.
[3] Hagberg DP, Edvinsson T, Marinado T, Boschloo G, Hagfeldt A, Sun L. A novel organic chromophore for dye-sensitized nanostructured solar cells. Chem Commun 2006;42:2245–7.
[4] Li S, Jiang KJ, Shao K, Yang L. Novel organic dyes for efficient dye-sensitized solar cells. Chem Commun 2006;42:2792–4.
[5] Ito S, Miura H, Uchida S, Takata M, Sumioka K, Liska P, et al. High-conversion-efficiency organic dye-sensitized solar cells with a novel indoline dye. Chem Commun 2008;44:5194–6.
[6] Bessho T, Zakeeruddin SM, Yeh CY, Diau EWG, Graetzel M. Highly efficient mesoscopic dye-sensitized solar cells based on donor–acceptor-substituted porphyrins. Angew Chem Int Ed 2010;49:6646–9.
[7] Zeng W, Cao Y, Bai Y, Wang Y, Shi Y, Zhang M, et al. Efficient dye-sensitized solar cells with an organic photosensitizer featuring orderly conjugated ethylenedioxythiophene and dithienosilole blocks. Chem Mater 2010;22:1915–25.
[8] Bai Y, Zhang J, Zhou D, Wang Y, Zhang M, Wang P. Engineering organic sensitizers for iodine-free dye-sensitized solar cells: red-shifted current response concomitant with attenuated charge recombination. J Am Chem Soc 2011;133:11442–5.
[9] Zhang F, Jiang K, Huang J, Yu C, Li S, Chen M, et al. A novel compact DPP dye with enhanced light harvesting and charge transfer properties for highly efficient DSCs. J Mater Chem A 2013;1:4858–63.
[10] Zhang GL, Bala H, Cheng YM, Shi D, Lv XJ, Yu QJ, et al. High efficiency and stable dye-sensitized solar cells with an organic chromophore featuring a binary π-conjugated spacer. Chem Commun 2009;45:2198–200.
[11] Huang J, Jiang K, Zhang F, Wu W, Li S, Yang L, et al. Engineering diketopyrrolopyrrole sensitizers for highly efficient dye-sensitized solar cells: enhanced light harvesting and intramolecular charge transfer. RSC Adv 2014;4:16906–12.
[12] Haid S, Marszalek M, Mishra A, Wielopolski M, Teuscher J, Moser JE, et al. Significant improvement of dye-sensitized solar cell performance by small structural modification in π-conjugated donor–acceptor dyes. Adv Funct Mater 2012;22:1291–302.
[13] Zhang GL, Bai Y, Li RZ, Shi D, Wenger S, Zakeeruddin SM, et al. Employ a bisthienothiophene linker to construct an organic chromophore for efficient and stable dye-sensitized solar cells. Energy Environ Sci 2009;2:92–5.
[14] Liu JY, Zhou DF, Xu MF, Jing XY, Wang P. The structure–property relationship of organic dyes in mesoscopic titania solar cells: only one double-bond difference. Energy Environ Sci 2011;4:3545–51.
[15] Xu MF, Zhang M, Pastore M, Li RZ, Angelis FD, Wang P. Joint electrical, photophysical and computational studies on D-π-A dye sensitized solar cells: the impacts of dithiophene rigidification. Chem Sci 2012;3:976–83.
[16] Cai N, Li RZ, Wang YL, Zhang M, Wang P. Organic dye-sensitized solar cells with a cobalt redox couple: influences of π-linker rigidification and dye-bath solvent selection. Energy Environ Sci 2013;6:139–47.
[17] Zhang M, Wang YL, Xu MF, Ma WT, Li RZ, Wang P. Design of high-efficiency organic dyes for titania solar cells based on the chromophoric core of cyclopentadithiophene-benzothiadiazole. Energy Environ Sci 2013;6:2944–9.
[18] Bijleveld JC, Zoombelt AP, Mathijssen SGJ, Wienk MM, Turbiez M, Leeuw DM, et al. Poly(diketopyrrolopyrrole–terthiophene) for ambipolar logic and photovoltaics. J Am Chem Soc 2009;131:16616–7.
[19] Qiao Z, Xu Y, Lin S, Peng J, Cao D. Synthesis and characterization of red-emitting diketopyrrolopyrrole-*alt*-phenylenevinylene polymers. Synth Met 2010;160:1544–50.
[20] Qu S, Tian H. Diketopyrrolopyrrole (DPP)-based materials for organic photovoltaics. Chem Commun 2012;48:3039–56.
[21] Fukuda M, Kodama K, Yamamoto H, Mito K. Evaluation of new organic pigments as laser-active media for a solid-state dye laser. Dyes Pigm 2004;63:115–25.
[22] Qu S, Wu W, Hua J, Kong C, Long Y, Tian H. New diketopyrrolopyrrole (DPP) dyes for efficient dye-sensitized solar cells. J Phys Chem C 2010;114:1343–9.
[23] Yum J, Holcombe TW, Kim Y, Rakstys K, Moehl T, Teuscher J, et al. Blue-coloured highly efficient dye-sensitized solar cells by implementing the diketopyrrolopyrrole chromophore. Sci Rep 2013;3:2446–53.
[24] Holcombe TW, Yum JH, Yoon J, Gao P, Marszalek M, Di Censo D, et al. A structural study of DPP-based sensitizers for DSC applications. Chem Commun 2012;48:10724–6.
[25] Qu SY, Qin CJ, Islam A, Wu YZ, Zhu WH, Hua JL, et al. A novel D–A-p-A organic sensitizer containing a diketopyrrolopyrrole unit with a branched alkyl chain for highly efficient and stable dye-sensitized solar cells. Chem Commun 2012;48:6972–4.
[26] Yum JH, Holcombe TW, Kim Y, Yoon J, Rakstys K, Nazeeruddin MK, et al. Towards high-performance DPP-based sensitizers for DSC applications. Chem Commun 2012;48:10727–9.
[27] Qu SY, Wang B, Guo FL, Li J, Wu WJ, Kong C, et al. New diketo-pyrrolo-pyrrole (DPP) sensitizer containing a furan moiety for efficient and stable dye-sensitized solar cells. Dyes Pigm 2012;92:1384–93.
[28] Becke AD. Density-functional thermochemistry. III. The role of exact exchange. J Chem Phys 1993;98:5648–52.
[29] Lee C, Yang W, Parr RG. Development of the Colle-Salvetti correlation-energy formula into a functional of the electron density. Phys Rev B 1988;37:785–9.
[30] Petersson GA, Al-Laham MA. A complete basis set model chemistry. II. Open-shell systems and the total energies of the first-row atoms. J Chem Phys 1991;94:6081–8.
[31] Frisch MJT, Schlegel HB, Scuseria GE, Robb MA, Cheeseman JR, Scalmani G, et al. Gaussian 09 (Revision A.1). Wallingford CT: Gaussian, Inc.; 2009.
[32] Cossi M, Rega N, Scalmani G, Barone V. Energies, structures, and electronic properties of molecules in solution with the C-PCM solvation model. J Comput Chem 2003;24:669–81.
[33] Yanai T, Tew DP, Handy NC. A new hybrid exchange–correlation functional using the Coulomb-attenuating method (CAM-B3LYP). Chem Phys Lett 2004;393:51–7.

[34] Yakhanthip T, Jungsuttiwong S, Namuangruk S, Kungwan N, Promarak V, Sudyoadsuk T, et al. Theoretical investigation of novel carbazole-fluorene based D-π-A conjugated organic dyes as dye-sensitizer in dye-sensitized solar cells (DSCs). J Comput Chem 2011;32:1568–676.
[35] Perdew JP, Burke K, Ernzerhof M. Generalized gradient approximation made simple. Phys Rev Lett 1996;77:3865–8.
[36] Perdew JP, Chevary JA, Vosko SH, Jackson KA, Pederson MR, Singh DJ, et al. Atoms, molecules, solids, and surfaces: applications of the generalized gradient approximation for exchange and correlation. Phys Rev B Condens Matter 1992;46:6671–87.
[37] Delley B. An all-electron numerical method for solving the local density functional for polyatomic molecules. J Chem Phys 1990;92:508–13.
[38] Delley B. From molecules to solids with the DMol3 approach. J Chem Phys 2000;113:7756–64.
[39] O'Boyle NM, Tenderholt AL, Langner KM. cclib: a library for package-independent computational chemistry algorithms. J Comput Chem 2008;29:839–45.
[40] Zhou N, Prabakaran K, Lee B, Chang SH, Harutyunyan B, Guo P, et al. Metal-free tetrathienoacene sensitizers for high-performance dye-sensitized solar cells. J Am Chem Soc 2015;137:4414–23.
[41] Lee KM, Lin LC, Suryanarayanan V, Wu CG. Titanium dioxide coated on titanium/stainless steel foil as photoanode for high efficiency flexible dye-sensitized solar cells. J Power Sources 2014;269:789–94.
[42] Li S, Jiang K, Zhang F, Huang J, Li S, Chen M, et al. New diketopyrrolopyrrole-based organic dyes for highly efficient dye-sensitized solar cells. Org Electron 2014;15:1579–85.
[43] Wu Y, Zhu W. Organic sensitizers from D–p–A to D–A–p–A: effect of the internal electron-withdrawing units on molecular absorption, energy levels and photovoltaic performances. Chem Soc Rev 2013;42:2039–58.
[44] Chen CY, Pootrakulchote N, Chen M, Moehl T, Tsai H, Zakeeruddin SM, et al. A new heteroleptic ruthenium sensitizer for transparent dye-sensitized solar cells. Adv Energy Mater 2012;2:1503–9.
[45] Raga SR, Barea EM, Santiago FF. Analysis of the origin of open circuit voltage in dye solar cells. J Phys Chem Lett 2012;3:1629–34.
[46] Pastore M, Fantacci S, De Angelis F. Modeling excited states and alignment of energy levels in dye-sensitized solar cells: successes, failures, and challenges. J Phys Chem C 2013;117:3685–700.
[47] De Angelis F, Fantacci S, Mosconi E, Nazeeruddin MK, Grätzel M. Absorption spectra and excited state energy levels of the N719 dye on TiO_2 in dye-sensitized solar cell models. J Phys Chem C 2011;115:8825–31.
[48] Li G, Liang M, Wang H, Sun Z, Wang L, Wang Z, et al. Significant enhancement of open-circuit voltage in indoline-based dye-sensitized cells via retarding charge recombination. Chem Mater 2013;25:1713–22.
[49] Scholes GD, Rumbles G. Excitons in nanoscale systems. Nat Mater 2006;5:683–97.